Research Article Vol. 1, No. 6 / December 2014 / Optica 436

Temporal, spectral, and polarization dependence of the nonlinear optical response of carbon disulfide

Matthew Reichert,[1] Honghua Hu,[1] Manuel R. Ferdinandus,[1,2] Marcus Seidel,[1] Peng Zhao,[1] Trenton R. Ensley,[1] Davorin Peceli,[1] Jennifer M. Reed,[1] Dmitry A. Fishman,[1] Scott Webster,[1] David J. Hagan,[1,3] and Eric W. Van Stryland[1,3,*]

[1]CREOL, College of Optics and Photonics, University of Central Florida, Orlando, Florida 32816, USA

[2]Department of Engineering Physics, Air Force Institute of Technology, Dayton, Ohio 45433, USA

[3]Department of Physics, University of Central Florida, Orlando, Florida 32816, USA

*Corresponding author: ewvs@creol.ucf.edu

Received 9 September 2014; revised 28 October 2014; accepted 31 October 2014 (Doc. ID 221494); published 18 December 2014

Carbon disulfide is the most popular material for applications of nonlinear optical (NLO) liquids, and is frequently used as a reference standard for NLO measurements. Although it has been the subject of many investigations, determination of the third-order optical nonlinearity of CS_2 has been incomplete. This is in part because of several strong mechanisms for nonlinear refraction (NLR), leading to a complex pulse width dependence. We expand upon the recently developed beam deflection technique, which we apply, along with degenerate four-wave mixing and Z-scan, to quantitatively characterize (in detail) the NLO response of CS_2, over a broad temporal range, spanning 6 orders of magnitude (~32 fs to 17 ns). The third-order response function, consisting of both nearly instantaneous bound-electronic and noninstantaneous nuclear contributions, along with the polarization and wavelength dependence from 390 to 1550 nm, is extracted from these measurements. This paper provides a self-consistent, quantitative picture of the third-order NLO response of liquid CS_2, establishing it as an accurate reference material over this broad temporal and spectral range. These results allow prediction of the outcome of any NLR experiment on CS_2.

OCIS codes: (190.4400) Nonlinear optics, materials; (300.6420) Spectroscopy, nonlinear; (190.3270) Kerr effect; (320.7110) Ultrafast nonlinear optics.

http://dx.doi.org/10.1364/OPTICA.1.000436

1. INTRODUCTION

Carbon disulfide (CS_2) is a widely used nonlinear optical (NLO) liquid owing to its large third-order nonlinear refraction (NLR). It has been subject to many experimental studies utilizing time-resolved techniques such as optical Kerr effect (OKE) [1–8], degenerate four-wave mixing (DFWM) [9,10], and nonlinear interferometry [11], as well as frequency domain light scattering [12–14], third-harmonic generation [15], and Z-scan [16–21]. It is found in a wide array of NLO applications, including liquid-core optical fibers for nonlinear photonics applications [22,23], soliton propagation [24,25], supercontinuum generation [26], slow light [27], ultrafast time-resolved imaging [28], and all-optical switching [29]. In addition, it is commonly used as a reference material for nonlinear spectroscopy [15,30,31]. However, the NLO response of CS_2 varies by more than 1 order of magnitude, over the time range of ~30 fs to ~30 ps [17]. This is because CS_2 exhibits a strong noninstantaneous third-order response,

arising from motions of the molecules. Two-photon absorption (2PA) also begins to play an important role in the nonlinear response for wavelengths shorter than 500 nm [32], and via Kramers–Kronig relations the bound-electronic component of the NLR displays dispersion in this region [33]. Without broad and accurate characterization of the pulse width and wavelength dependence of its nonlinearity, the use of CS_2 as a calibration material is problematic.

Many of the previous time-domain measurements of CS_2 have focused solely on relative magnitudes (and dynamics) of the nuclear response, and provide no information on the absolute magnitude of the nonlinearity [1,5,6,9,10,34]. Other time domain investigations have used a relative measurement technique, and compared their results to literature values of the nonlinearity of a reference material [11]. Reports of quantitative measurements of NLR, using absolutely calibrated techniques (such as Z-scan), only pertain to specific pulse widths and wavelengths, and are thus limited in applicability.

In this paper, we present a thorough experimental investigation of the third-order NLO response of CS_2. By applying our newly developed beam deflection (BD) technique [35], we measure the third-order temporal response function, including the absolute magnitude and symmetry of each component, without a need to scale to a reference material. The BD method is particularly useful, for measuring the absolute magnitudes of the various nonlinear mechanisms, by displaying the temporal dynamics and polarization dependence. We then apply the measured response function to predict the results of additional independent NLO experiments: DFWM and Z-scans, with pulses from 32 fs to 17 ns, including linear and circular polarizations. Additionally, we determine the dispersion of NLR, including both bound-electronic and nuclear contributions, and the spectrum of 2PA from 390 to 1550 nm. These data give a self-consistent, quantitative picture of the third-order nonlinear dynamics of liquid CS_2, making possible a prediction of the outcome of any measurement of 2PA or NLR.

2. ORIGINS OF NONLINEAR REFRACTION IN CS_2

Several mechanisms give rise to a change in the refractive index of CS_2, each with its own characteristic response time and polarization dependence. Within the Born–Oppenheimer approximation, these mechanisms may be divided into two categories: those of the bound electrons, and those of the nuclei. The bound-electronic contribution to the third-order response originates from the purely electronic second hyperpolarizability of the individual molecules. The response time is limited by the time–energy uncertainty relation, to typically <1 fs, which is essentially instantaneous compared to the pulse duration, and is related to the transition dipole coupling between discrete electronic states of the molecule. The characteristic response times of the nuclear mechanisms to the index change are approximately hundreds of fs, owing to the large mass of the nuclei. These nuclear motions give rise to a third-order optical response, by altering the bulk linear susceptibility $\chi^{(1)}$, either through a change in the molecular polarizability, or by changes in the average orientation of the molecular ensemble. Each contribution to the third-order response causes an irradiance, and time-dependent change in the refractive index, which for a single beam is given by

$$\Delta n(t) = n_{2,el} I(t) + \int_{-\infty}^{\infty} R(t - t') I(t') \mathrm{d}t', \tag{1}$$

where $I(t)$ is the irradiance, $R(t)$ is the noninstantaneous component of the third-order response, and $n_{2,el}$ is the nonlinear refractive index that originates from the bound electrons. All experiments are outside the linear absorption regime, and thus

$$n_{2,el} = \frac{3\,\mathrm{Re}(\chi^{(3)})}{4 n_0^2 \varepsilon_0 c}, \tag{2}$$

where n_0 is the linear refractive index, ε_0 the vacuum permittivity, $\chi^{(3)}$ the bound-electronic third-order susceptibility, and c is the speed of light in vacuum [15]. The first term of Eq. (1) describes the bound-electronic response and follows the temporal irradiance profile of the pulse, while the second term describes the change in refractive index due to the noninstantaneous nuclear motions. While there have been theoretical investigations of the effect of correlations of various nuclear motions on the third-order optical response [36,37], multiple investigators have found good agreement with experiments by treating these mechanisms as linearly independent [1,5,11]. We take the same approach here, and write the nuclear contribution as a sum of three responses:

$$R(t) = \sum_m n_{2,m} r_m(t), \tag{3}$$

where $n_{2,m}$ is the magnitude of the mth mechanism and the temporal response function $r_m(t)$ is normalized such that

$$\int_{-\infty}^{\infty} r_m(t) \mathrm{d}t = 1. \tag{4}$$

The dominant nuclear mechanism in CS_2 is molecular reorientation [38]. Due to its linear shape it exhibits anisotropic polarizability and has no permanent dipole moment. A strong electric field induces a dipole leading to an applied torque, causing the molecular axis to align with the incident field. The time scale of reorientation depends on the moment of inertia of the molecules, which are angularly accelerated by the electric field. After a sufficiently short pulse, the molecules will continue to orient toward the field and then thermally randomize at a rate that depends on the viscosity of the liquid. Since the diffusive nature of the relaxation follows the Debye–Stokes–Einstein relation [39], this mechanism is referred to as diffusive reorientation. The molecules may be modeled as a driven damped harmonic oscillator [1], where in the overdamped case the temporal response function is well-described by

$$r_d(t) = C_d \left(1 - e^{-\frac{t}{\tau_{r,d}}}\right) e^{-\frac{t}{\tau_{f,d}}} \Theta(t), \tag{5}$$

where the subscript d indicates the diffusive reorientation mechanism, $\tau_{r,d}$ and $\tau_{f,d}$ are the rise and fall times, respectively, $C_d = (\tau_{r,d} + \tau_{f,d})/\tau_{f,d}^2$ is a normalization factor, and $\Theta(t)$ is the Heaviside function which ensures causality.

In liquids, the interactions of neighboring molecules must be considered when looking at molecular motion. One example is libration, which is an oscillatory rocking motion resulting from a molecule aligning toward the electric field but hindered by the environment. The influence of this mechanism on the refractive index is due to the coherent oscillation of many molecules. Hence, a loss of coherence between many oscillators, caused by collisional dephasing, is the dominant decay mechanism of this induced index change [1]. The quantum harmonic oscillator model of the (underdamped) librational response function is given by [4]

$$r_l(t) = C_l e^{-\frac{t}{\tau_{f,l}}}\Theta(t)\int_0^\infty \frac{\sin(\omega t)}{\omega} g(\omega)\mathrm{d}\omega, \tag{6}$$

where the subscript l indicates the librational mechanism and $g(\omega)$ is the distribution function of libration frequencies. Since different molecules experience different environments within the liquid, this librational motion is inhomogeneously broadened [40]. We use the "antisymmetrized" Gaussian distribution function [14]

$$g(\omega) = e^{-\frac{(\omega-\omega_0)^2}{2\sigma^2}} - e^{-\frac{(\omega+\omega_0)^2}{2\sigma^2}}, \tag{7}$$

where ω_0 is the central frequency and σ is the spectral width.

Finally, there are intermolecular collision-induced variations in the molecular polarizability. One cause is dipole-induced dipole interactions, where in addition to the applied field, each molecule also experiences the reradiated electric field from the induced dipole in the neighboring molecules, which distorts its polarizability [41]. Electronic overlap effects become important for very small molecular separations [37,41]. Time domain measurements have found that the collision-induced mechanism follows an exponential rise and decay function [1,11,42]. The (overdamped) collision-induced contribution follows a response function of the form

$$r_c(t) = C_c\left(1 - e^{-\frac{t}{\tau_{r,c}}}\right)e^{-\frac{t}{\tau_{f,c}}}\Theta(t), \tag{8}$$

where the subscript c indicates the collision-induced mechanism. Similar responses have been observed in atomic liquids, including Ar and Xe [42], which have isotropic polarizabilities.

The four nonlinear mechanisms have two different polarization dependencies. Given the isotropic nature of the liquid at room temperature, the bound-electronic and collision-induced mechanisms follow isotropic symmetry. However, diffusive reorientation and libration have a quite different polarization dependence. As the CS_2 molecules align toward the electric field, anisotropy is generated within the liquid. The average polarizability, and thus refractive index, is increased in the direction of alignment and decreased in the perpendicular directions. We refer to this type of polarization dependence as reorientational. The isotropic and reorientational mechanisms may be easily isolated by conducting measurements with the appropriate polarizations. This gives an additional dimension to aid in the characterization of the third-order response of CS_2.

3. BEAM DEFLECTION

To fully characterize the temporal dynamics of CS_2, we make use of our recently developed BD technique [35]. As shown in Fig. 1, a strong excitation beam induces a change in the refractive index following its Gaussian spatial profile. The resulting index gradient is sensed by a weaker, and spatially smaller, probe beam aligned off center of the excitation beam where the irradiance gradient is maximized. Typically, the probe beam has a size ~5× smaller than that of the excitation beam. The prism-like index gradient induced by the excitation causes the probe to be deflected, as measured by a segmented quadcell detector in the far-field. The BD technique has distinct advantages over other nonlinear excite–probe techniques. It produces a signal that is linearly proportional to the induced refractive index change, directly giving its sign, and thus does not require optical heterodyne detection as OKE or DFWM. In addition, various tensor elements may be measured directly by altering the polarizations of the excitation and probe beams, whereas OKE measures the induced birefringence. BD is much easier to implement than two-color Z-scan [43] or interferometric techniques [11].

To eliminate experimental complications, such as coherent-coupling effects [5,44,45] and a large background signal from the excitation, we use different wavelengths for the excitation and probe. However, the relatively high dispersion of CS_2 [46] causes the pulses to propagate with different group velocities and pass through one another in time, resulting in a reduced signal [47]. Following Negres et al. [47], we develop a simple method of analysis for the BD measurements in the presence of group velocity mismatch (GVM) and a noninstantaneous nonlinear material response. This may be applied to any material in the limit where the pulse widths do not change upon propagation through the sample, i.e., negligible group velocity dispersion (GVD). In our experiments, pulses are estimated to broaden by less than 9% [46]. This analysis allows us to experimentally determine the third-order nonlinear response of CS_2, including absolute magnitudes of each

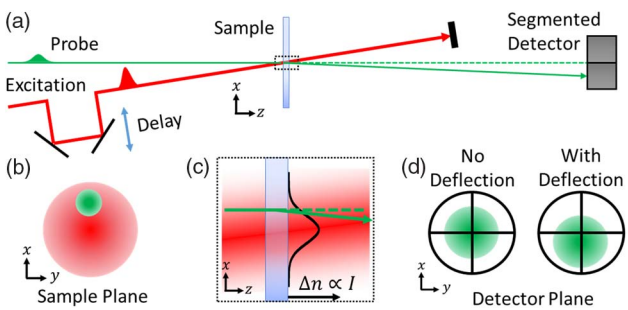

Fig. 1. (a) Schematic diagram of BD experiment [35]; (b) irradiance distribution of excitation (red), and probe (green) at sample plane; (c) zoom in of (a) at sample showing a profile of Δn; (d) probe beam on segmented detector without and with deflection.

mechanism, their characteristic response times, and polarization dependence.

Equation (9) gives the nonlinear wave equation for a weak probe centered at frequency ω in the limit of zero depletion of the excitation pulse at ω_e [48]. The sample is assumed to be thin, meaning the thickness is less than the Rayleigh range of both beams, and the peak induced phase changes are small [16]. This makes the excitation irradiance I_e independent of propagation distance z and the deflection of the probe within the sample negligible. The probe electric field is $\mathbf{E}(\mathbf{r},z,t) = 1/2\mathcal{E}(\mathbf{r},z,t)e^{i(kz-\omega t)}\hat{\mathbf{e}} + \text{c.c.}$, where $\mathcal{E}(\mathbf{r},z,t)$ is the field amplitude, $\mathbf{r}$ is the radial coordinate, $k = \omega n_0/c$ is the wave number and $\hat{\mathbf{e}}$ is the electric field unit vector.

$$i\left(\frac{\partial}{\partial z} + \frac{1}{v}\frac{\partial}{\partial t}\right)\mathcal{E} + k_0\mathcal{E}\left(2n_{2,el}I_e(t) + \int_{-\infty}^{\infty} R(t-t')I_e(t')\mathrm{d}t'\right) = 0, \tag{9}$$

where $k_0 = \omega/c$ and v is the probe group velocity (see Supplement 1 for derivation). The second term of Eq. (9) represents the nonlinear interaction of the probe pulse with the excitation. It is written as the sum of the bound-electronic contribution (plus the convolution of the excitation pulse), with the noninstantaneous nuclear component of the third-order response function. The factor within the parentheses is $\Delta n(t)$, experienced by the weak probe, induced by the excitation. Note the instantaneous component, $2n_{2,el}I_e(t)$, is greater by a factor of 2 than that in Eq. (1). The excitation and probe fields interfere, and generate a refractive index grating, off which the excitation diffracts into the probe direction (and vice versa), with the appropriate phase and amplitude to double the phase shift, so called weak-wave retardation [44,49]. This is true even in the nondegenerate case, since the instantaneous bound-electronic response is able to follow the rapidly moving grating. The noninstantaneous nuclear component, however, is too slow to follow the grating, and no additional phase shift appears [44]. In the degenerate case, this grating is stationary, or very slowly moving for chirped pulses, and the noninstantaneous response does contribute additional terms to the nonlinear interaction [45]. Equation (9) assumes the nondegenerate case $\omega_e \neq \omega$.

Following [47], the solution for Gaussian pulses with the addition of the noninstantaneous third-order response, and the transverse spatial profiles of the excitation and probe, is given by

$$\mathcal{E}(\mathbf{r},T) = \mathcal{E}_0(\mathbf{r})\exp\left(-\frac{(T+T_d-\rho)^2}{2\mathcal{T}^2} + i\frac{k_0L}{\rho}I_{e,0}(\mathbf{r})\cdot\left\{2n_{2,el}[\mathrm{erf}(T)-\mathrm{erf}(T-\rho)] + \int_{T-\rho}^{T}\int_{-\infty}^{\infty} R(T_2-T_1)e^{-T_1^2}\mathrm{d}T_1\mathrm{d}T_2\right\}\right), \tag{10}$$

where $T = (t - z/v_e)/\tau_e$ is the dimensionless normalized time (that moves with the excitation group velocity v_e), τ_e is the excitation pulse width (HW1/eM), T_d is the dimensionless delay between excitation and probe, $\mathcal{T} = \tau/\tau_e$ is the normalized probe pulse width, and L is the sample thickness. The GVM parameter is

$$\rho = \frac{L}{\tau_e}\left(\frac{1}{v} - \frac{1}{v_e}\right) = \frac{L}{\tau_e c}(n_g - n_{g,e}), \tag{11}$$

where n_g and $n_{g,e}$ are group indices of the probe and excitation, respectively. Equation (10) describes the propagation of a weak probe pulse accounting for both instantaneous and noninstantaneous nonlinear effects induced by the excitation, as well as temporal walk-off due to GVM. We implement Fresnel diffraction of the probe field from the back of the sample to the quad-cell detector. The BD signal is then calculated as the difference in energy detected on the left-half side of the quad-cell, minus that on the right-half side [35].

In typical excite–probe experiments where GVM is neglected, the temporal resolution is limited by the width of the cross correlation of the excitation and probe pulses. GVM causes the two pulses to overlap at different distances within the sample at different time delays, which results in a broadening and smoothing of the measured signal as a function of delay [50]. The temporal resolution of a given experiment is no longer only a parameter of the apparatus, but depends on the dispersion of the material under investigation. One consequence of this broadening is a reduction of the temporal resolution of the noninstantaneous response.

4. TIME DOMAIN EXPERIMENTS

BD is used to measure the magnitude, time constants, and polarization dependence of each nonlinear mechanism that contributes to the third-order response. The experimental setup consists of slight modifications to a standard excite–probe experiment (Fig. 1) and is the same as that reported in [35]. A commercial Ti:sapphire chirped-pulse-amplifier system (Coherent Legend Duo+) with 12 mJ output energy at 800 nm, with a bandwidth of 28 nm at a repetition rate of 1 kHz, is used to produce the excitation pulse of duration 50 fs (temporal durations are given in FWHM unless otherwise specified), as determined from autocorrelation measurements. The probe pulse is generated by splitting off a portion of the excitation pulse and focusing it into a 1 cm cuvette filled with water to create a white-light continuum, from which a central wavelength of 650 nm is filtered out using a narrow bandpass interference filter. Both the pulses have Gaussian spatial profiles. The pulse energy of each beam is controlled via a combination of half-wave plates and polarizers. The probe beam is focused to a beam waist of $w = 38$ μm(HW1/e^{2}M) at the sample, and the excitation is focused to $w_e = 170$ μm. The excitation beam is then horizontally displaced from the probe beam by $w_e/2$ to maximize the deflection angle. The crossing angle between the beam is kept small, <2°, to prevent spatial walk-off within the sample. The deflection of the probe is measured by an OSI QD50-0-SD quad-segmented silicon photodiode positioned 17 cm behind the sample. The quad-cell detector is initially centered on the probe beam. The excitation induces

a deflection in the probe, causing it to shift on the detector and yield a difference in energy on the left and right segments, $\Delta E = E_{\text{left}} - E_{\text{right}}$. The total energy falling on all four segments, E, is measured simultaneously, and serves both for normalization and as a monitor for nonlinear absorption, which we do not observe. Both ΔE and E are lock-in detected at the 286 Hz chopping frequency of the excitation beam, and are measured as a function of delay between the two pulses. For a sample with only instantaneous third-order NLR, $\Delta E/E$ is proportional to the cross correlation of the pulses. The pulse width of the probe is determined from a BD measurement of fused silica to be 158 fs. All measurements on CS_2 (Sigma-Aldrich, 270660, ≥99.9%) are conducted using 1 mm path length, fused silica cuvettes. Using the refractive index measurements of [46], we find $\rho = 4.7$.

The refractive index change seen by the probe depends on the relative angle θ of its linear polarization with respect to that of the excitation. The induced index change may be described by the index ellipsoid [38], which for small changes simplifies to

$$\Delta n(\theta) = \Delta n_{\parallel} \cos^2(\theta) + \Delta n_{\perp} \sin^2(\theta). \tag{12}$$

The relation between $\Delta n_{\parallel}$ and $\Delta n_{\perp}$ depends on the polarization dependence of the responsible mechanisms. For third-order nonlinearities with isotropic symmetry, $\Delta n_{\perp}^{\text{iso}} = \Delta n_{\parallel}^{\text{iso}}/3$, and for reorientational, $\Delta n_{\perp}^{\text{re}} = -\Delta n_{\parallel}^{\text{re}}/2$. We may therefore write the polarization dependence of the refractive index change as [35]

$$\Delta n(\theta) = \Delta n_{\parallel}^{\text{iso}} \left(\cos^2(\theta) + \frac{1}{3} \sin^2(\theta) \right) + \Delta n_{\parallel}^{\text{re}} \left(\cos^2(\theta) - \frac{1}{2} \sin^2(\theta) \right). \tag{13}$$

The reorientational term is eliminated at the so called "magic angle" ($\theta = \arctan\sqrt{2} \approx 54.7°$), leaving only the isotropic component [6]. BD measurements are conducted at three polarization angles of the probe beam, with respect to the excitation ($\theta = 0°$, parallel; 90°, perpendicular; and 54.7°, magic angle), which is adjusted using a half-wave plate that is calibrated with a polarizer. For theses angles

$$\begin{aligned} \Delta n(0°) &= \Delta n_{\parallel}^{\text{iso}} + \Delta n_{\parallel}^{\text{re}}, \\ \Delta n(90°) &= \frac{1}{3}\Delta n_{\parallel}^{\text{iso}} - \frac{1}{2}\Delta n_{\parallel}^{\text{re}}, \\ \Delta n(54.7°) &= \frac{5}{9}\Delta n_{\parallel}^{\text{iso}}. \end{aligned} \tag{14}$$

The BD data is fit using Eq. (10). We begin at the magic angle, since it isolates the isotropic components and allows unambiguous determination of their magnitudes and time constants. As shown in Fig. 2, the signal at the magic angle is dominated by the bound-electronic mechanism but also exhibits a small noninstantaneous contribution consistent with other observations [6,7,10]. We attribute this

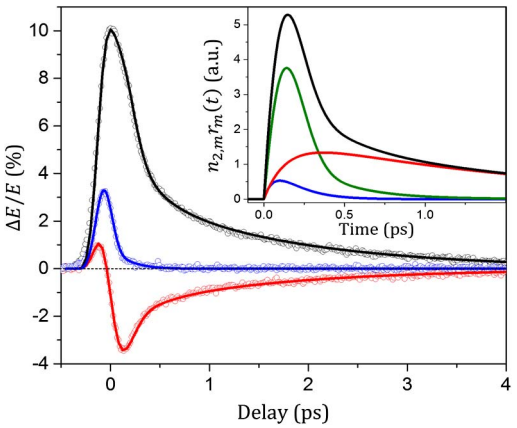

Fig. 2. Measured (circles) and fit (curves) BD signals for parallel (black), magic angle (blue), and perpendicular (red) polarizations; inset shows the resultant noninstantaneous responses of collision (blue), diffusive reorientation (red), libration (green), and their sum (black).

noninstantaneous contribution to the collision-induced nuclear mechanism [6], due to its symmetry and fit with Eq. (8). The magnitudes are scaled by 9/5 to give $\Delta n_{\parallel}^{\text{iso}}$ [Eq. (14)], which is then applied to the measurements with parallel and perpendicular polarizations, which show two additional noninstantaneous components corresponding to the libration and diffusive reorientation mechanisms. These are fit with Eqs. (5) and (6), respectively. We do not resolve the rise times for the collision-induced and diffusive reorientation mechanisms, and therefore follow [1], and assume them to be equal since inertial delay should influence each similarly. The best fit of both parallel and perpendicular polarization data sets is used to determine the final values given in Table 1. Errors in $n_{2,m}$ are estimated from the uncertainty in irradiance (~20%) and the signal-to-noise ratio. Those for the remaining parameters are determined in the fitting procedure by varying a single component until the curves no longer match the data. Our results agree well with previous measurements using similar models but here include absolute magnitudes as well as response times [1,4,5,9,34]. Using Eq. (2), $\chi^{(3)}_{xxxx} = (1.8 \pm 0.4) \times 10^{-21}\ \text{m}^2/\text{V}^2$ [$(1.3 \pm 0.3) \times 10^{-13}$ esu], and $\chi^{(3)}_{xyxy} = \chi^{(3)}_{xyyx} = \chi^{(3)}_{xxyy} = (\chi^{(3)}_{xxxx}/3) = (0.6 \pm 0.1) \times 10^{-21}\ \text{m}^2/\text{V}^2$ [$(0.4 \pm 0.1) \times 10^{-13}$ esu].

Using these results we are then able to predict the results of a DFWM experiment. This was conducted using another Ti:sapphire chirped-pulse-amplifier (Clark-MXR CPA 2010) with 1 mJ output energy at a repetition rate of 1 kHz, which pumps an optical parametric amplifier (Light Conversion, TOPAS-C) tuned to 700 nm. A prism compressor (SF10)

Table 1. Fit Parameters of Third-Order Response of CS_2[a]

Mechanism	$n_{2,m}$	$\tau_{r,m}$ (fs)	$\tau_{f,m}$ (fs)	Symmetry
Electronic	2.0 ± 0.4	Instantaneous		iso
Collision	1.0 ± 0.2	150 ± 50	140 ± 50	iso
Libration	7.6 ± 1.5	[b]	450 ± 100	re
Diffusive	18 ± 3	150 ± 50	1610 ± 50	re

[a] $n_{2,m}$ are given in units of $10^{-19}\ \text{m}^2/\text{W}$.
[b] $\omega_0 = 8.5 \pm 1.0\ \text{ps}^{-1}$ and $\sigma = 5 \pm 1\ \text{ps}^{-1}$.

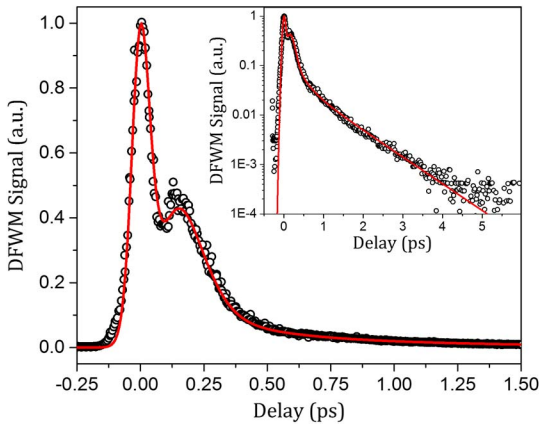

Fig. 3. Normalized DFWM signal of CS_2 (circles), and calculation (curve) using the response function model values of Table 1; inset shows logarithmic scale.

compresses the pulse, which is then split by a 50/50 beamsplitter, and the reflected pulse is sent to a delay line. The two beams are overlapped onto a transmissive diffraction grating. The ± 1 diffracted orders of the top beam act as the excitation, and the $+1$ order of the bottom beam acts as a probe. The two excitation beams are focused and overlapped in the CS_2 and generate a refractive index grating off of which the probe beam diffracts [9,10]. The measured signal is proportional to the diffraction efficiency, which is related to the square of the induced refractive index change. The prism compressor is adjusted to yield the narrowest signal in delay. Figure 3 shows the normalized DFWM signal versus delay along with a simulation of the experiment using the response function with the values in Table 1 for 88 and 42 fs pulse widths of the excitation and probe pulses, respectively. The calculation shows excellent agreement with the experimental data, validating the results obtained with the BD technique, and demonstrates our ability to apply the measured response function to predict the outcome of other NLO experiments on CS_2.

5. Z-SCAN EXPERIMENTS

CS_2 is often used as a reference material for Z-scan experiments despite its pulse width dependent NLR. From the measured third-order response function the effective nonlinear refractive index, defined by $\Delta n = n_{2,\mathrm{eff}} I$, can be calculated and compared to Z-scan experiments. Defining $n_{2,\mathrm{eff}}$ in this way is commonly done but does not address the dynamics of the physical processes that cause the index change and results in pulse width dependent values. To check our predictions of $n_{2,\mathrm{eff}}$, we conduct Z-scans at both 700 and 1064 nm, over a broad range of pulse widths by using a prism compressor/stretcher. The same commercial Ti:sapphire laser system used for the DFWM experiments is also used here. The experimental setup has been described previously [16]. The prism compressor is used to vary the pulse duration from 32 fs (corresponding to the bandwidth limit) to 2.3 ps (limited by available space in the setup). The beam is then spatially filtered to produce a Gaussian beam. A small portion ($\sim$10%) of the beam is split off to a reference detector to window the pulse energy, which is controlled by a half-wave plate and polarizer. A quarter-wave plate is inserted before the focusing lens for circular polarization measurements. A beam splitter after the sample allows both open aperture (OA) and closed aperture (CA) Z-scans, which are sensitive to NLA and NLR, respectively, to be performed simultaneously. A mode-locked Nd:YAG laser system (EKSPLA PL2143) operating at 10 Hz is also used to measure $n_{2,\mathrm{eff}}$ with ps pulses. In addition to the 1064 nm laser output itself, which had a pulse width of 25 ± 1 ps, it is also frequency tripled and used to pump an OPG/A, which is tuned to 700 nm with a pulse width of 8 ± 1 ps. For all measurements the thin sample approximation is valid [16,51].

OA Z-scan measurements of 2PA in ZnSe for 700 nm (with 2PA coefficient $\alpha_2 = 5.6 \times 10^{-11}$ m/W [52]), and CdSe for 1064 nm ($\alpha_2 = 23 \times 10^{-11}$ m/W [52]), and CA Z-scan measurements of fused silica ($n_{2,el} = 0.25 \times 10^{-19}$ m^2/W [53]) are used to determine the spot size and pulse width by fitting with the standard Z-scan analysis [16]. Determining the pulse width and spot size in this manner minimizes the relative error between Z-scans at different pulse widths. Z-scans of CS_2 are performed at multiple energies to ensure the linear dependence of the peak-to-valley transmission change with irradiance, and the best fit to all curves is used to determine the value of $n_{2,\mathrm{eff}}$ (see Supplement 1).

The Z-scan technique is sensitive to changes of the material's refractive index, which are only proportional to $n_{2,el}$, in the case of an instantaneous response. Therefore, an irradiance-weighted time average has to be performed in order to map the BD results on the pulse width dependent $n_{2,\mathrm{eff}}$ values determined from the Z-scan measurements. The time averaged index change over the duration of the pulse is [16]

$$\langle \Delta n(t) \rangle = \frac{\int \Delta n(t) I(t) \mathrm{d}t}{\int I(t) \mathrm{d}t}. \tag{15}$$

For a response assumed to be instantaneous

$$\langle \Delta n(t) \rangle = n_{2,\mathrm{eff}} \frac{\int I^2(t) \mathrm{d}t}{\int I(t) \mathrm{d}t}. \tag{16}$$

Equating Eqs. (15) and (16), using Eq. (1) for $\Delta n(t)$, and solving for $n_{2,\mathrm{eff}}$, yields

$$n_{2,\mathrm{eff}} = n_{2,el} + \frac{\int I(t) \int R(t - t') I(t') \mathrm{d}t' \mathrm{d}t}{\int I^2(t) \mathrm{d}t}. \tag{17}$$

Figure 4 shows the measured values of $n_{2,\mathrm{eff}}$ from Z-scans using linear polarization to those calculated using Eq. (17). Measurements at both 700 and 1064 nm overlap, demonstrating the negligible dispersion of the noninstantaneous contribution to the NLR. In the limit of short pulses, $n_{2,\mathrm{eff}} = n_{2,el}$, since only the bound-electronic response contributes. As the pulse width increases, the noninstantaneous contributions add to $n_{2,\mathrm{eff}}$, which plateaus for pulses longer

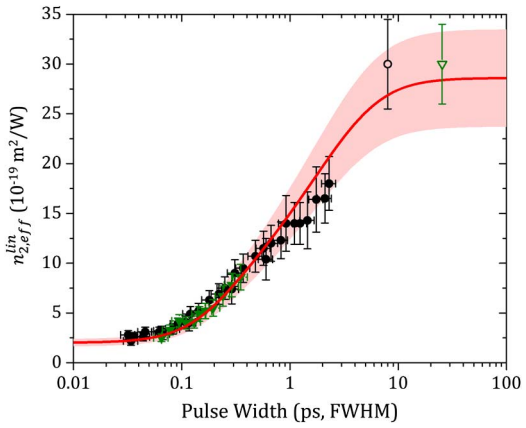

Fig. 4. Comparison of Z-scan measurements (see Supplement 1) using the Ti:sapphire (closed) and Nd:YAG laser system (open), at both 700 nm (black) and 1064 nm (green), and calculation using Eq. (17), red curve, of $n_{2,\mathrm{eff}}$, of CS_2 versus pulse width; shaded region represents errors in the response function from Table 1.

than ~10 ps. In this long-pulse limit $n_{2,\mathrm{eff}}$ is given by the sum of each component's magnitude:

$$n_{2,\mathrm{eff}}|_{\mathrm{long}} = \sum_m n_{2,m}. \tag{18}$$

Our results agree with the BD predictions, using the values of Table 1, and with other Z-scan measurements of $n_{2,\mathrm{eff}}$ [16–21,54]. Z-scan measurements are also performed using circular polarization. The ratio of $n_{2,\mathrm{eff}}$ for linear and circular polarizations, $n_{2,\mathrm{eff}}^{\mathrm{lin}}/n_{2,\mathrm{eff}}^{\mathrm{circ}}$, is an indication of the polarization dependence of the underlying mechanisms. For materials possessing isotropic symmetry, this ratio is 1.5, while for reorientational mechanisms it is 4 [38]. In CS_2, $n_{2,\mathrm{eff}}^{\mathrm{lin}}/n_{2,\mathrm{eff}}^{\mathrm{circ}}$ depends on the pulse duration. By using the symmetry properties of the response function, we find $\Delta n_{\mathrm{circ}} = \Delta n_{\parallel}^{\mathrm{iso}}/1.5 + \Delta n_{\parallel}^{\mathrm{re}}/4$. Figure 5 shows excellent agreement between the measured values $n_{2,\mathrm{eff}}^{\mathrm{lin}}/n_{2,\mathrm{eff}}^{\mathrm{circ}}$ versus pulse width and that predicted by

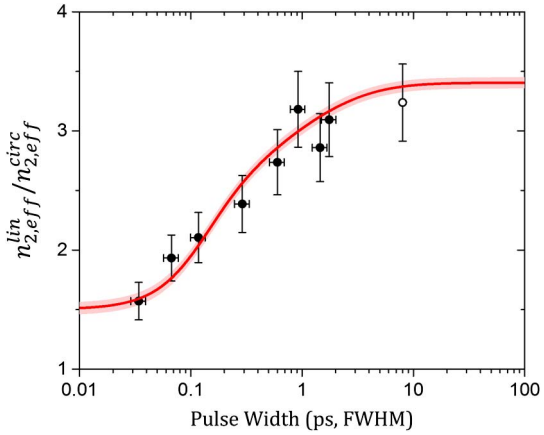

Fig. 5. Comparison of $n_{2,\mathrm{eff}}^{\mathrm{lin}}/n_{2,\mathrm{eff}}^{\mathrm{circ}}$ versus pulse width between Z-scan measurements with both Ti:sappire (closed circles) and Nd:YAG (open circle) laser systems at 700 nm and calculated (red curve); shaded region represents only relative errors that contribute to uncertainty.

the third-order response function in Table 1. In the short pulse limit, $n_{2,\mathrm{eff}}^{\mathrm{lin}}/n_{2,\mathrm{eff}}^{\mathrm{circ}} = 1.5$ because it is dominated by the isotropic bound-electronic response, while in the long pulse limit this ratio becomes

$$\left.\frac{n_{2,\mathrm{eff}}^{\mathrm{lin}}}{n_{2,\mathrm{eff}}^{\mathrm{circ}}}\right|_{\mathrm{long}} = \frac{n_{2,\mathrm{eff}}^{\mathrm{lin}}|_{\mathrm{long}}}{\frac{(n_{2,el}+n_{2,c})}{1.5} + \frac{(n_{2,I}+n_{2,d})}{4}}, \tag{19}$$

where the numerator is given by Eq. (18), and the denominator shows the weighting of each contribution according to its polarization dependence. Using the results in Table 1, for long pulse widths $n_{2,\mathrm{eff}}^{\mathrm{lin}}/n_{2,\mathrm{eff}}^{\mathrm{circ}} = 3.4$.

To study the dispersion of the bound-electronic component of the third-order response, we conduct Z-scans at several wavelengths from 390 to 1550 nm, at the shortest pulse widths achievable. Depending on the wavelength, the minimum pulse width varies from 32 to 165 fs. Over this range, the nonlinearity of CS_2 is dominated by the bound-electronic response, but the noninstantaneous component can still contribute significantly, and can increase $n_{2,\mathrm{eff}}$ up to ~2×. However, if we assume the nuclear response is independent of wavelength, we can calculate its contribution for each particular pulse width, and simply subtract it out. That is, since we know $R(t)$ from the BD measurements, and we measure $n_{2,\mathrm{eff}}$ with a Z-scan, we can calculate $n_{2,el}$ using Eq. (17). To verify our assumption, we perform Z-scans using long pulses, both with the ps system as well as a 10 Hz Q-switched Nd:YAG (Continuum PL9010) ns system, pumping an optical parametric oscillator (Continuum Sunlite EX), that produces pulses from 2.5 to 16.5 ns, depending on the wavelength. For ns pulses, electrostriction can also contribute to the closed aperture Z-scan signal, and analysis is done to extract its contribution [54]. Figure 6(a) shows $n_{2,\mathrm{eff}}|_{\mathrm{long}}$ is independent of wavelength to within the measurement uncertainty. Since the nuclear components dominate for long pulses, we conclude that they have negligible dispersion. Therefore, for the short pulse measurements we may subtract the nuclear contribution to $n_{2,\mathrm{eff}}$ from the value measured via Z-scan, and isolate only the bound-electronic contribution.

Figure 6(b) shows both the dispersion of $n_{2,el}$ with the nuclear contribution removed and the spectrum of α_2. A quantum mechanical perturbation approach, known as the "sum over states" (SOS) model, which considers all electronic dipole allowed transitions between various states, is used to determine the NLO response [55]. In this way $n_{2,el}$ and α_2 can be calculated from knowledge of the energies of the electronic states and their respective transition dipole moments μ. Here, we use only three states in the model [56,57]: the ground state, a one-photon allowed state e, and a 2PA final state e'. Due to the symmetry of the molecule, the states g and e' have the same parity and thus $\mu_{ge'} = 0$. The results are shown in Table 2. Parameters for state e were found by measuring the linear absorption spectrum of a 0.445 mM solution of CS_2 in methanol. The reported transition dipole moments are vacuum values, i.e., they have been corrected for local field effects [38]. The corresponding spectral shape of $n_{2,el}$ agrees well with the experimental data both in peak position and trend of

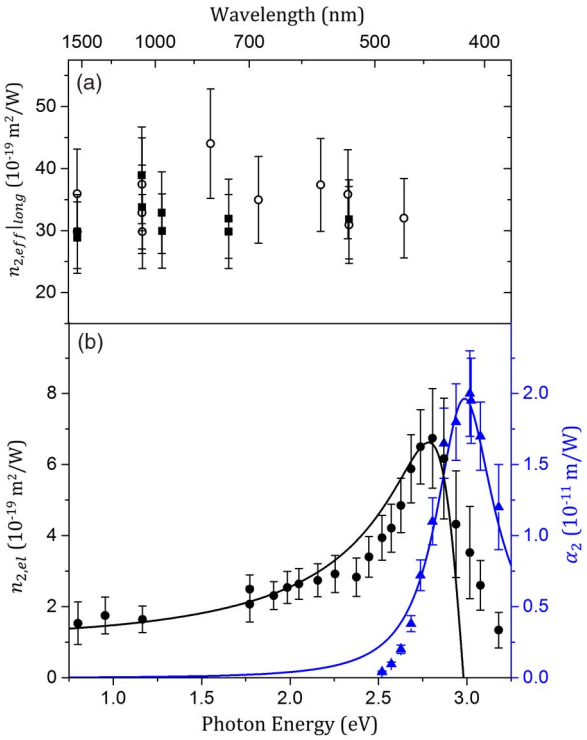

Fig. 6. (a) Z-scan measurements of dispersion of $n_{2,\text{eff}}|_{\text{long}}$ for (open circles) 13 to 20 ps and (closed squares) 2.5 to 17 ns, with the electrostriction contribution subtracted; (b) Z-scan measurements of NLR (black circles) for fs pulses with noninstantaneous component subtracted and α_2 (blue triangles); curves represent the SOS model fit for 2PA (blue) and $n_{2,el}$ (black), which has been multiplied by a factor of 2.

Table 2. Fit Parameters for SOS Model of $n_{2,el}$ and α_2 of CS_2

State	Energy (eV)	HWHM (eV)	μ (D)
e	6.00 ± 0.01	0.17 ± 0.01	$\mu_{ge} = 3.6 \pm 0.2$
e'	5.95 ± 0.05	0.40 ± 0.05	$\mu_{ee'} = 8.7 \pm 0.9$

variation. However, it underestimates the magnitude by a factor of 2, which may be a consequence of the simplicity of the model. Using these parameters, the SOS model may be applied to predict the values of $\chi^{(3)}$ for other optical frequencies (e.g., third harmonic generation (THG) [15]).

6. CONCLUSION

By the application of several measurement techniques, we have experimentally investigated the third-order NLO response of CS_2 to give a complete picture of its temporal, polarization, and spectral dependence. Using the recently developed BD technique [35], we have measured the absolute magnitude of the third-order response function. We have expanded the analysis of the BD technique to include a noninstantaneous component of NLR and GVM. A model of instantaneous bound-electronic and three non-instantaneous nuclear responses, i.e., collision, libration, and diffusive reorientation, is found to give excellent agreement with the BD experimental data. The polarization dependence of each mechanism is used to determine their respective tensor symmetries. Calculations of the results of DFWM using the BD generated response function give excellent agreement with experimental results.

Based on the measured response function, we are able to predict the pulse width dependent $n_{2,\text{eff}}$, which agrees very well with Z-scan measurements over a range from 32 fs to 17 ns. For long pulses slower effects also contribute to the refractive index change, including electrostriction (ns) and thermal effects (ms), which have been well-characterized previously [54,58]. With the polarization dependence of the various response mechanisms, predicted results of Z-scans, conducted with both linear and circular polarizations, also give excellent agreement with experimental results. Since the dispersion of the nuclear mechanisms is shown to be negligible, the dispersion of the bound-electronic response is isolated in short-pulse Z-scan measurements. The dispersion of $n_{2,el}$ and the spectrum of 2PA across a broad wavelength range (from 390 to 1550 nm) is presented. This allows analysis in terms of a simplified quantum mechanical model that matches the spectral shape.

We are therefore able to predict the nonlinearity of CS_2 over a broad range of experimental parameters. This paper will prove useful for those making use of CS_2 for a multitude of NLO applications including as a reference material for NLO spectroscopy. The experimental approach demonstrated here may be applied to a wide variety of other materials for robust quantitative determination of the temporal, spectral, and polarization dependence of their NLO response.

FUNDING INFORMATION

Air Force Office of Scientific Research (AFOSR) (FA9550-10-1-0558); National Science Foundation (NSF) (ECCS-1202471, ECCS-1229563).

ACKNOWLEDGMENT

The authors thank Lazaro A. Padilha, Mihaela Balu, and Gero Nootz for their motivating work.

See Supplement 1 for supporting content.

REFERENCES

1. D. McMorrow, W. T. Lotshaw, and G. A. Kenney-Wallace, "Femtosecond optical Kerr studies on the origin of the nonlinear responses in simple liquids," IEEE J. Quantum Electron. **24**, 443–454 (1988).
2. P. P. Ho and R. R. Alfano, "Optical Kerr effect in liquids," Physical Review A **20**, 2170–2187 (1979).
3. K. Kamada, "Mechanisms of ultrafast refractive index change in organic system," Proc. SPIE **4797**, 65–75 (2003).
4. D. McMorrow, N. Thantu, V. Kleiman, J. S. Melinger, and W. T. Lotshaw, "Analysis of intermolecular coordinate contributions to third-order ultrafast spectroscopy of liquids in the harmonic oscillator limit," J. Phys. Chem. A **105**, 7960–7972 (2001).
5. T.-H. Huang, C.-C. Hsu, T.-H. Wei, S. Chang, S.-M. Yen, C.-P. Tsai, R.-T. Liu, C.-T. Kuo, W.-S. Tse, and C. Chia, "The transient optical Kerr effect of simple liquids studied with an ultrashort laser with variable pulsewidth," IEEE J. Sel. Top. Quantum Electron. **2**, 756–768 (1996).
6. S. Constantine, J. A. Gardecki, Y. Zhou, L. D. Ziegler, X. Ji, and B. Space, "A novel technique for the measurement of

polarization-specific ultrafast Raman responses," J. Phys. Chem. A **105**, 9851–9858 (2001).
7. C. J. Fecko, J. D. Eaves, and A. Tokmakoff, "Isotropic and anisotropic Raman scattering from molecular liquids measured by spatially masked optical Kerr effect spectroscopy," J. Chem. Phys. **117**, 1139–1154 (2002).
8. N. T. Hunt, A. A. Jaye, and S. R. Meech, "Polarisation-resolved ultrafast Raman responses of carbon disulfide in solution and microemulsion environments," Chem. Phys. Lett. **371**, 304–310 (2003).
9. T. Steffen and K. Duppen, "Time resolved four- and six-wave mixing in liquids. II. Experiments," J. Chem. Phys. **106**, 3854–3864 (1997).
10. Q.-H. Xu, Y.-Z. Ma, and G. R. Fleming, "Heterodyne detected transient grating spectroscopy in resonant and non-resonant systems using a simplified diffractive optics method," Chem. Phys. Lett. **338**, 254–262 (2001).
11. Y. Sato, R. Morita, and M. Yamashita, "Study on ultrafast dynamic behaviors of different nonlinear refractive index components in CS_2 using a femtosecond interferometer," Jpn. J. Appl. Phys. **36**, 2109–2115 (1997).
12. S. L. Shapiro and H. P. Broida, "Light scattering from fluctuations in orientations of CS_2 in liquids," Phys. Rev. **154**, 129–138 (1967).
13. N. Bloembergen and P. Lallemand, "Complex intensity-dependent index of refraction, frequency broadening of stimulated Raman lines, and stimulated Rayleigh scattering," Phys. Rev. Lett. **16**, 81–84 (1966).
14. J. S. Friedman and C. Y. She, "The effects of molecular geometry on the depolarized stimulated gain spectra of simple liquids," J. Chem. Phys. **99**, 4960–4969 (1993).
15. I. Rau, F. Kajzar, J. Luc, B. Sahraoui, and G. Boudebs, "Comparison of Z-scan and THG derived nonlinear index of refraction in selected organic solvents," J. Opt. Soc. Am. B **25**, 1738–1747 (2008).
16. M. Sheik-Bahae, A. A. Said, T. H. Wei, D. J. Hagan, and E. W. Van Stryland, "Sensitive measurement of optical nonlinearities using a single beam," IEEE J. Quantum Electron. **26**, 760–769 (1990).
17. R. A. Ganeev, A. I. Ryasnyansky, M. Baba, M. Suzuki, N. Ishizawa, M. Turu, S. Sakakibara, and H. Kuroda, "Nonlinear refraction in CS_2," Appl. Phys. B **78**, 433–438 (2004).
18. X.-Q. Yan, X.-L. Zhang, S. Shi, Z.-B. Liu, and J.-G. Tian, "Third-order nonlinear susceptibility tensor elements of CS_2 at femtosecond time scale," Opt. Express **19**, 5559–5564 (2011).
19. M. Falconieri and G. Salvetti, "Simultaneous measurement of pure-optical and thermo-optical nonlinearities induced by high-repetition-rate, femtosecond laser pulses: application to CS_2," Appl. Phys. B **69**, 133–136 (1999).
20. S. Couris, M. Renard, O. Faucher, B. Lavorel, R. Chaux, E. Koudoumas, and X. Michaut, "An experimental investigation of the nonlinear refractive index (n2) of carbon disulfide and toluene by spectral shearing interferometry and Z-scan techniques," Chem. Phys. Lett. **369**, 318–324 (2003).
21. I. P. Nikolakakos, A. Major, J. S. Aitchison, and P. W. E. Smith, "Broadband characterization of the nonlinear optical properties of common reference materials," IEEE J. Sel. Top. Quantum Electron. **10**, 1164–1170 (2004).
22. K. Kieu, L. Schneebeli, R. A. Norwood, and N. Peyghambarian, "Integrated liquid-core optical fibers for ultra-efficient nonlinear liquid photonics," Opt. Express **20**, 8148–8154 (2012).
23. S. Pricking, M. Vieweg, and H. Giessen, "Influence of the retarded response on an ultrafast nonlinear optofluidic fiber coupler," Opt. Express **19**, 21673–21679 (2011).
24. E. L. Falcão-Filho, C. B. de Araújo, G. Boudebs, H. Leblond, and V. Skarka, "Robust two-dimensional spatial solitons in liquid carbon disulfide," Phys. Rev. Lett. **110**, 013901 (2013).
25. S. Pricking and H. Giessen, "Generalized retarded response of nonlinear media and its influence on soliton dynamics," Opt. Express **19**, 2895–2903 (2011).
26. D. Churin, T. N. Nguyen, K. Kieu, R. A. Norwood, and N. Peyghambarian, "Mid-IR supercontinuum generation in an integrated liquid-core optical fiber filled with CS_2," Opt. Mater. Express **3**, 1358–1364 (2013).
27. O. D. Herrera, L. Schneebeli, K. Kieu, R. A. Norwood, and N. Peyghambarian, "Slow light based on stimulated Raman scattering in an integrated liquid-core optical fiber filled with CS_2," Opt. Express **21**, 8821–8830 (2013).
28. H. Purwar, S. Idlahcen, C. Rozé, D. Sedarsky, and J.-B. Blaisot, "Collinear, two-color optical Kerr effect shutter for ultrafast time-resolved imaging," Opt. Express **22**, 15778–15790 (2014).
29. S. Sahu, R. R. Pal, and S. Dhar, "Nonlinear material based all-optical parallel subtraction scheme: an implementation," Int. J. Optoelectron. **1**, 7–11 (2011).
30. M. Moran, S. Chiao-Yao, and R. Carman, "Interferometric measurements of the nonlinear refractive-index coefficient relative to CS_2 in laser-system-related materials," IEEE J. Quantum Electron. **11**, 259–263 (1975).
31. M. R. Ferdinandus, M. Reichert, T. R. Ensley, H. Hu, D. A. Fishman, S. Webster, D. J. Hagan, and E. W. Van Stryland, "Dual-arm Z-scan technique to extract dilute solute nonlinearities from solution measurements," Opt. Mater. Express **2**, 1776–1790 (2012).
32. D. Kong, Q. Chang, Y. Gao, H. A. Ye, L. Zhang, G. Shi, X. Zhang, Y. Wang, K. Yang, and Y. Song, "Nonlinear absorption of CS_2 at the wavelength of 400 nm with femtosecond pulses," Physica B **407**, 1279–1281 (2012).
33. D. C. Hutchings, M. Sheik-Bahae, D. J. Hagan, and E. W. Stryland, "Kramers-Krönig relations in nonlinear optics," Opt. Quantum. Electron. **24**, 1–30 (1992).
34. T. Steffen, N. A. C. M. Meinders, and K. Duppen, "Microscopic origin of the optical Kerr effect response of CS_2–pentane binary mixtures," J. Phys. Chem. A **102**, 4213–4221 (1998).
35. M. R. Ferdinandus, H. Hu, M. Reichert, D. J. Hagan, and E. W. Van Stryland, "Beam deflection measurement of time and polarization resolved ultrafast nonlinear refraction," Opt. Lett. **38**, 3518–3521 (2013).
36. K. Kiyohara, K. Kamada, and K. Ohta, "Orientational and collision-induced contribution to third-order nonlinear optical response of liquid CS_2," J. Chem. Phys. **112**, 6338–6348 (2000).
37. D. Kivelson and P. Madden, "Light scattering studies of molecular liquids," Ann. Rev. Phys. Chem. **31**, 523–558 (1980).
38. R. W. Boyd, *Nonlinear Optics*, 3rd ed. (Academic/Elsevier, 2008).
39. P. Debye, *Polar Molecules* (Dover, 1929).
40. C. Kalpouzos, D. McMorrow, W. T. Lotshaw, and G. A. Kenney-Wallace, "Femtosecond laser-induced optical Kerr dynamics in CS_2/alkane binary solutions," Chem. Phys. Lett. **150**, 138–146 (1988).
41. J. A. Bucaro and T. A. Litovitz, "Rayleigh scattering: collisional motions in liquids," J. Chem. Phys. **54**, 3846–3853 (1971).
42. B. I. Greene, P. A. Fleury, H. L. Carter, and R. C. Farrow, "Microscopic dynamics in simple liquids by subpicosecond birefringences," Phys. Rev. A **29**, 271–274 (1984).
43. M. Sheik-Bahae, J. Wang, R. DeSalvo, D. J. Hagan, and E. W. Van Stryland, "Measurement of nondegenerate nonlinearities using a two-color Z scan," Opt. Lett. **17**, 258–260 (1992).
44. J. K. Wahlstrand, J. H. Odhner, E. T. McCole, Y. H. Cheng, J. P. Palastro, R. J. Levis, and H. M. Milchberg, "Effect of two-beam coupling in strong-field optical pump-probe experiments," Phys. Rev. A **87**, 053801 (2013).
45. A. Dogariu, T. Xia, D. J. Hagan, A. A. Said, E. W. Van Stryland, and N. Bloembergen, "Purely refractive transient energy transfer by stimulated Rayleigh-wing scattering," J. Opt. Soc. Am. B **14**, 796–803 (1997).
46. A. Samoc, "Dispersion of refractive properties of solvents: chloroform, toluene, benzene, and carbon disulfide in ultraviolet, visible, and near-infrared," J. Appl. Phys. **94**, 6167–6174 (2003).
47. R. A. Negres, J. M. Hales, A. Kobyakov, D. J. Hagan, and E. W. Van Stryland, "Experiment and analysis of two-photon absorption spectroscopy using a white-light continuum probe," IEEE J. Quantum Electron. **38**, 1205–1216 (2002).

48. G. P. Agrawal, *Nonlinear Fiber Optics*, 3rd ed. (Academic, 2001).
49. E. W. Van Stryland, A. L. Smirl, T. F. Boggess, M. J. Soileau, B. S. Wherrett, and F. A. Hopf, "Weak-wave retardation and phase-conjugate self-defousing in Si," in *Picosecond Phenomena III*, K. B. Eisenthal, R. M. Hochstrasser, W. Kaiser, and A. Laubereau, eds. (Springer, 1982), pp. 368–371.
50. M. Ziólek, M. Lorenc, and R. Naskrecki, "Determination of the temporal response function in femtosecond pump-probe systems," Appl. Phys. B **72**, 843–847 (2001).
51. A. E. Kaplan, "'External' self-focusing of light by a nonlinear layer," Radiophys. Quantum Electron. **12**, 692–696 (1969).
52. M. Sheik-Bahae, D. C. Hutchings, D. J. Hagan, and E. W. Van Stryland, "Dispersion of bound electron nonlinear refraction in solids," IEEE J. Quantum Electron. **27**, 1296–1309 (1991).
53. D. Milam, "Review and assessment of measured values of the nonlinear refractive-index coefficient of fused silica," Appl. Opt. **37**, 546–550 (1998).
54. D. I. Kovsh, S. Yang, D. J. Hagan, and E. W. Van Stryland, "Nonlinear optical beam propagation for optical limiting," Appl. Opt. **38**, 5168–5180 (1999).
55. B. J. Orr and J. F. Ward, "Perturbation theory of the non-linear optical polarization of an isolated system," Mol. Phys. **20**, 513–526 (1971).
56. M. G. Kuzyk and C. W. Dirk, "Effects of centrosymmetry on the nonresonant electronic third-order nonlinear optical susceptibility," Phys. Rev. A **41**, 5098–5109 (1990).
57. H. Hu, "Third order nonlinearity of organic molecules," Ph. D. dissertation (University of Central Florida, 2012).
58. D. Kovsh, D. Hagan, and E. Van Stryland, "Numerical modeling of thermal refraction in liquids in the transient regime," Opt. Express **4**, 315–327 (1999).